RSC Advances

ROYAL SOCIETY OF CHEMISTRY

www.rsc.org/advances

{110} facets predominated $Bi_6O_6(OH)_3(NO_3)_3 \cdot 1.5H_2O$ photocatalyst: selectively hydrothermal synthesis and superior photocatalytic activity for degradation of phenol

Li-Min Yang, Guo-YingZhang*, Yue Liu*, Yan-Yan Xu, Chun-Mei Liu, Jing-Wang Liu

Tianjin Key Laboratory of Structure and Performance for Functional Molecules; Key Laboratory of Inorganic-Organic Hybrid Functional Material Chemistry, Ministry of Education; College of Chemistry, Tianjin Normal University, Tianjin 300387, China

* Corresponding author. Tel./fax: +86 22 23766532

*E-mail address:*hxxyzgy@mail.tjnu.edu.cn (G.-Y. Zhang);

hxxyly@mail.tjnu.edu.cn(Y. Liu)

Abstract: The basic bismuth (III) nitrate photocatalyst with composition of $Bi_6O_6(OH)_3(NO_3)_3 \cdot 1.5H_2O$ (BBN) was facilely synthesized by hydrothermal strategy *via* incomplete hydrolysis of bismuth nitrate. The characterizations of composition, morphology, microstructure, optical absorption, BET, and photocatalytic behavior were systematically explored. The results indicate that the BBN architectures built up of multilayered meshing-tooth with predominated {110} side facets can be selectively obtained by fine-tuning the reaction parameters. The sample exhibits obviously superior photocatalytic activity for degradation of phenol compared with BBN sheets of dominant top {001} planes and commercial P25 with rate constant *k* improved by 3.6 and 2.8 folds, respectively. The excellent photocatalytic behavior combined with its rather low BET surface area of 0.0453 $m^2 \cdot g^{-1}$ indicates the highly reactive {110} facets in BBN for photocatalysis. The active oxidation species and main intermediates in phenol/BBN system are ascertained by scavenger experiments and high performance liquid chromatography (HPLC) technique. Combine the band edge of BBN and the redox potentials of active species, the possible migration mechanism of photogenerated e^-/h^+ pairs on the surface of BBN is proposed. This work provides some new insights for the rational design and synthesis of active-facet exposed basic salt photocatalyst with excellent efficiency.

Keywords: Selective synthesis; $Bi_6O_6(OH)_3(NO_3)_3 \cdot 1.5H_2O$; Photocatalysis; Active facets; Carrier migration; Intermediates

1. Introduction

Phenol and its derivatives are categorized as one of the most serious environmental contaminants discharged by industrial plants due to their toxicity, carcinogenicity and difficulty to degrade.[1,2] In recent years, semiconductor photocatalysis has gradually become one of the most effective technologies in the degradation of phenolic wastewater since it can completely treat the pollutants to harmless end products under mild conditions.[3-6] The key issue for the photocatalytic degradation of phenol contaminants in wastewater depends on the performance of photocatalytic materials used. Developing a new efficient photocatalyst to meet future environmental requirement is still one of the focuses of current studies.

Among the numerous semiconductors, bismuth-contained materials have been received great attention in environmental remediation over the past few years. Bismuth (Bi) is a *p*-block metal with a d^{10}configuration, and the Bi 6s orbitals can interact with the O 2p orbitals to form a preferable hybridized valence band (VB), which favors the mobility of photogenerated holes in the VB and benefits the enhancement of the photocatalytic performance of the Bi^{3+}-based oxides.[7] So far, bismuth compounds with satisfactory photocatalytic properties for the degradation of organic pollutants are gradually researched in the photocatalytic field such as Bi_2O_3[8,9], Bi_2WO_6[10,11], Bi_2MoO_6[12,13], $BiVO_4$[14,15], BiOX (X=Cl, Br, I)[16-18], and *etc*. Bi-based basic salt is another family member of bismuth compounds and it has shown very rich crystal chemistry with almost 15 different structures discovered.[19] They were preliminarily studied for medical application and as precursor for bismuth oxides,[20]

and seldom attention has been given in the domain of photocatalysis.

Just recently, the basic bismuth nitrate nanosheets with complex composition of $Bi_6O_6(OH)_3(NO_3)_3 \cdot 1.5H_2O$ was found to be a new type of photocatalyst for UV-light degradation of dyes such as malachite green and methyl orange.[21,22] But for nanosized photocatalyst, it is difficult to be thoroughly recollected from the degradation solution and thus brings about secondary pollution. And organic dyes can often be seriously degraded under UV illumination even in the absence of photocatalyst. Our recent research has shown that BBN is also an efficient co-catalyst of Bi_2WO_6 for degradation of Rhodamine B due to band-gap coupling effect.[23] Although double-layered BBN architecture has been synthesized by Liu *et al.* for removal of phenol but only exhibited comparable UV photocatalytic activity with classic P25.[24] In the very limited reports, no systematical exploration has been carried out to clarify the influence of preparation parameters on the structure, which is a prerequisite for better understanding of the relationship between the specific structure and photocatalytic performance. Usually, the photocatalytic reaction occurs at the interface of the reactant and catalyst, and the photocatalytic activity is strongly dependent on the surface morphology and exposed crystal facets.[25-27] Pioneering works on the synthesis of anatase[28,29] and BiOCl[30,31] with highly reactive facets have paved a new way for the enhancement of photocatalytic performance. Undoubtedly, facet engineering not only is an exciting direction to pursue for highly active new-generation photocatalysts but also offers opportunities to investigate the relationship between the surface properties and the photocatalytic properties.

In this paper, we first report on the controllable synthesis of BBN architectures built up of multilayered tooth-meshing with predominated {110} side surface and the facet-dependent photoreactivity for degradation of phenol under UV light. The {110} facets predominated BBN photocatalyst exhibits obviously superior photocatalytic activity to less layered counterparts and individual BBN sheets with dominant {001} crystal planes. And it also presents much higher photocatalytic behavior than P25 with a rate constant improved by 2.8 folds. The migration direction of photoinduced carriers at the reaction interface is further provided based on the results of active species and intermediates.

2. Experimental section

Preparation

All the reagents were of analytical grade and used without further purification. BBN with predominant {110} facets was prepared as follows: 1mmol $Bi(NO_3)_3 \cdot 5H_2O$ was dissolved in 17.0 mL distilled water. After stirred for 30 min, the resulting suspension was transferred into a 25 mL Teflon-lined stainless steel autoclave and heated at 120 **℃** for 8 h. After the autoclave cooled to room temperature naturally, the solid products were collected by centrifugation, washed repeatedly with deionized water and absolute ethanol for several times, and then dried at 60 ℃ in air. For comparison, a series of parallel experiments was designed. All temperature series samples were treated from 80 to 200 ℃ for 8 h and time series samples were prepared at 120 ℃ for different hours, keeping other conditions unchanged (Tab. S1).

Characterization

The crystal phase and composition of the samples were characterized by X-ray diffraction (XRD) on a Bruker D8-Advance diffractometer with Cu Kα (λ = 0.15418 nm) radiation. Morphologies and microstructures of the prepared products were examined with a field-emission scanning electron microscopy (FEI, NOVA Nano SEM 230) and a high-resolution transmission electron microscopy (FEI, Tecnai G^2 F20). BET surface area measurement was obtained through N_2 adsorption-desorption isotherms collected at liquid nitrogen temperature using a Micromeritics ASAP2020 surface area and porosity analyzer. The UV-vis diffuse reflectance spectra were recorded on a JASCO V-550/V-570 UV-vis spectrophotometer fitted with an integrating sphere accessory.

Photocatalytic tests

Photocatalytic activities of the samples were evaluated for the degradation of phenol aqueous solution under UV irradiation (300W Hg lamp) in a photoreactor equipped with water circulation facility (Fig. S1). In each test, 10.0 mg of photocatalyst was added into phenol solution with the initial concentration of 10^{-4} M in a quartz tube. Before illumination, the suspension was magnetically stirred in dark for 30 min to establish an adsorption-desorption equilibrium. Then at given time intervals, one quartz tube was taken out and the photocatalyst was immediately separated by centrifugation to analyze the supernate by a Shimadzu 2550 UV-vis spectrophotometer.

The degradation intermediates of phenol were monitored with HPLC of Agilent 1100 series (Palo Alto, CA, USA) equipped with an Agilent Zorbax Eclipse

XDB-C18 column (150 mm × 4.6 mm, 5μm). During the sample analysis, the column was maintained at 30 °C. The intermediates were detected in an isocratic elution program. Methanol and water with volume ratio of 30:70 were used as mobile phase at a flow-rate of 1 mL/min and the injection volume was 20 μL.

3. Results and discussions

Phase, morphology and microstructure analysis

Fig.1 shows the typical XRD pattern of the hydrothermal sample selectively prepared at 120 °C for 8 h. All diffraction peaks match well with those of tetragonal basic bismuth (III) nitrate BBN ($a = b = 3.818$ Å, $c = 17.149$ Å, JCPDS: 53-1038). No sights of impurity phases such as Bi, $BiO(NO_3)$, Bi_2O_3,and $Bi(NO_3)_3$ are detected, showing the high purity of the product. And the sharp and narrow diffraction peaks indicate the high crystallinity of BBN. But it is interestingly noted that the intensity ratios of the diffraction peaks show obviously difference with that of the standard values. The (002) peak is greatly inhibited but the (110) and (102) peaks are dramatically strengthened. In particular, the diffraction intensity ratio of (110)/(002) planes in the as-obtained BBN sample is 2.5, promoted by 25 folds compared with the standard value of 0.1. And the intensity ratio of (102)/(002) has also been enhanced by 12.2 times. The XRD result demonstrates the preferential growth of specific crystal plane in BBN.

The morphology and microstructure of BBN are identified by SEM and TEM. The panoramic SEM image in Fig.2a indicates that the sample consists of monodispersed globular-like structure mostly ranging from 20 to 37 μm in diameter with coarse

surface. The close-up view of a few BBN architectures in Fig.2b shows that the spheres are built up of multilayered tooth-meshing of 10-15 layers. The coarse surface comes from the ragged arrangement of triangle-shaped tooth with side length of 1-3 μm. Further investigation was carried out by TEM to give detailed insights into the microstructures of BBN. The cog-wheel outline of an isolated BBN particle shown in the TEM image (Fig.2c) agrees well with the tooth-meshing structure as indicated in SEM. Fig.2d shows the HRTEM image of the edge part projected from the top surface of a BBN meshing-tooth. Clear lattice fringe with spacing of 0.270 nm corresponds to {110} crystal planes and implies the high crystallinity of the meshing-tooth. The selected-area electron diffraction (SAED) in Fig.2e with well-ordered dot pattern further confirms the single crystal nature of the building unit and can be well indexed to {110} equivalent planes. The ED pattern was projected from the [001] zone axis of a BBN meshing-tooth. Therefore, the exposed side surface of the tooth structure is dominant {110} facets, while the top surface of the tooth unit belongs to {001} facets. The TEM data coupled with XRD result strongly confirm that the BBN sample with multi-layered meshing-tooth exhibits predominated {110} crystal planes.

Influence of preparation parameters

To gain a better understanding of the formation process of the BBN superstructures, products obtained at different growth stages were collected for SEM and XRD measurement. As shown in Fig.3a, the precursor presents orderly rods with length of 10-25 μm and width of 2-5 μm, respectively. As the reaction proceeds for 30 min (Fig. 3b), the rods become disordered and tend to construct into a few clusters. After 50

min of reaction, some multilayered tooth-meshing architectures have appeared with the coexistence of precursor rods and transitional clusters. The fast transformation from clusters to tooth-meshing superstructure may disclose the metastable property of the intermediate morphology. The XRD patterns show that the products before 50 min are complex and difficult to be indexed due to the complicated hydrolysis of bismuth nitrate.[32] After 2 h of treatment, the rods and clusters disappear completely and all the particles present tooth-meshing structure but with much less layers and non-uniform diameters. At this stage, the XRD pattern can be ascribed to tetragonal BBN and the (110) and (102) peaks have showed preferential growth compared with the standard file. Finally, BBN architectures of well-defined multilayered tooth-meshing are formed *via* the Ostwald ripening process[33] at 8h. And the prevailed (110) diffraction has been in sharp contrast to the great inhibition of (002) peak. It seems that the more exposed side faces in the multilayered meshing-tooth structures account for the obvious change in facet orientation. And it has been ascertained by HRTEM that the side surface belongs to {110} planes.

The influences of hydrothermal temperature on the morphology and structure of BBN were also investigated. As shown in Fig.4a, the sample obtained at 80 ℃ is still randomly constructed rods with complicated XRD pattern. At elevated temperature of 100-120 ℃, the samples are distinguished from the former with morphologies of multilayered tooth-meshing (Fig.4b-c). But the architectures formed at 120 ℃ are more uniform and have obviously more layers of meshing-tooth. Although the BBN products both exhibit preferential (110) planes, vivid comparison gives a 1.3-fold

higher intensity ratio of (110)/(002) planes at 120 °C. Further increase of hydrothermal temperature leads to great changes in both morphology and structure. As shown in Fig.4d, the compact BBN architectures become cracked with 3D meshing-tooth gradually replaced by flatted sheets at 160 °C. And the corresponding XRD pattern gives an obviously strengthened (002) diffraction peak. At a high temperature of 200 °C, the BBN architectures have been seriously destroyed, accompanied by the growth of isolated and irregular sheets with lateral size of 20-40 μm. And the XRD pattern displays predominant (002) peak with a ratio of (002)/(110) approaching the standard value. The results further indicate that the exposed side surface of the meshing-tooth should be mainly attributed to {110} facets. So appropriate hydrothermal temperature and time are both key factors to achieve BBN structures with preferentially oriented {110} facets.

Optical properties

To confirm the optical absorption property of the BBN architectures, UV-vis DRS spectrum was measured with the result shown in Fig.5. According to the spectrum, the BBN presents the photoabsorption to UV light with a threshold of 375 nm. The steep shape of the spectrum indicates that the light absorption is not due to the transition from the impurity level but comes from the intrinsic band-gap transition.[34] Thus the BBN with composition of $Bi_6O_6(OH)_3(NO_3)_3 \cdot 1.5H_2O$ behaves like a bulk semiconductor. For a crystalline semiconductor, the optical absorption near the band edge follows the equation $\alpha h\nu = A(h\nu - Eg)^{n/2}$, where α, $h\nu$, A, and E_g are the absorption coefficient, photonic energy, proportionality constant, and band gap,

respectively.[35] And the value of *n* decides the characteristics of the transition in a semiconductor.[36] According to previous literature[24] and the clear region of linearity in $(\alpha hv)^{1/2}$ vs. hv, the value of *n* for BBN is ascertained to be 4 as indirect transition. As can be expected based on the absorption spectra, the sample is white in color. The intercept of the tangent to the plot gives a good approximation of the band gap energy of 3.3 eV. The DRS spectrum indicates that the BBN can be used as a photocatalyst under UV irradiation.

Photocatalytic properties

The photocatalytic degradation of phenol over temperature and time series samples was evaluated under the irradiation of a 300 W Hg lamp with results shown in Fig.6. The contrast test shows that only ca. 6.5 % of phenol was degraded in the dark in the presence of BBN, indicating that the adsorption of phenol can be negligible. The blank test in the absence of BBN presents reversely raised absorption at 270 nm in the initial stage (Fig. S2). The phenomenon has been reported in the study of UV photolysis of phenol and it is ascribed to the excessively accumulated intermediates with similar structure to phenol.[37] The slightly decreased absorbance after 60 min irradiation in the absence of BBN shows the ineffectiveness of direct photolysis. The BBN sample prepared at 120 °C for 8h gives the best photocatalytic behavior with 98.1% removal of phenol in 45 min, which is much better than commercial P25 under the same conditions. As shown in Fig. 6b, the pseudo first-order kinetics constants *k* of the phenol degradation over BBN is calculated to be 0.08945 min^{-1}, improved by a factor of 2.8 in comparison with that of P25 (0.03192 min^{-1}). It should be noted that

the BET surface area of BBN is detected merely 0.045 $m^2 \cdot g^{-1}$, which is considerably smaller than 43.26 $m^2 \cdot g^{-1}$ of the most widely used P25. The superior photocatalytic activity and rather low surface area may suggest the preferential orientation of reactive facets in BBN. The as-obtained sample also exhibits higher degradation efficiency than the reported double-layered BBN architecture.[24] For example, 38% of phenol has been degraded after 15 min irradiation over the multilayered BBN in compared with the value of only 6.0% over double-layered BBN. And there is still 18% of phenol left after 45 min photocatalysis for double-layered BBN in contrast to the little residue of 1.9% in our work. The results may imply the important role of the side face of the BBN meshing-tooth in photocatalysis, which is further confirmed by the following photocatalytic results over temperature and time series BBN samples.

The hydrothermal temperature has a significant influence on the photocatalytic activity of BBN. As shown in Fig.6a-b, the degradation of phenol increases at first and then decreases with the improvement of temperature, and the best activity is achieved at 120 °C. Its rate constant *k* is as fast as 2.4 and 3.6 times of BBN samples obtained at 100 and 200 °C, respectively. From the above SEM and XRD analysis, it is known that the BBN-120 °C presents the most layers of meshing-tooth with predominated {110} side surfaces. However, the BBN-200 °C exhibits prevailed microsheets with extremely diminished side faces but dominant {100} top surfaces. And the BET surface area of the sheet-shaped BBN is 0.245 $m^2 \cdot g^{-1}$, which is 5.4-folds higher than that of BBN-120 °C. The much improved photocatalytic activity combined with the lowered surface area confirms the high reactivity of the

predominated {110} facets in BBN-120 ℃. Fig.6c-d shows that reaction time is another important factor for the photocatalytic activity of BBN. The 50-min sample gives a rather low photocatalytic activity due to the partial formation of tooth-meshing architectures as shown in Fig.4. The degradation of phenol is accelerated over BBN for prolonged hydrothermal time with more layers of meshing-tooth. But a conversely lowered activity was detected for BBN-12h with a rate constant *k* only 34% of that of BBN-8h. The structure and morphology analysis (Fig.S3) imply that BBN-12h shows decreased layers of meshing-tooth and much inhibited (110) planes. The results further confirm the highly reactive {110} tooth surface of BBN.

Effects of process parameters

The photocatalytic performance of a catalyst is affected by various process parameters. The influences of BBN dosage and initial concentration of phenol solution were investigated. As shown in Fig.7a, the degradation efficiency of phenol is firstly increased and then decreased with the enhancement of BBN amount and the best BBN dosage is fixed at 10 mg. The corresponding rate constant *k* (inset) over 10 mg of BBN is improved by 3.5 and 3.0 times compared with that of 5 and 20 mg of BBN, respectively. Obviously, lower catalytic activity is observed when a smaller amount of catalyst is used because less catalytic active sites are available. However, excessive BBN powder would cause an increase in the opacity of the degradation solution and light scattering and even a decrease in the number of catalytic surface active sites caused by aggregation of photocatalyst particles.[38] So there is often an optimum amount of photocatalyst to achieve the maximum photocatalytic efficiency.

And this phenomena have also been reported in previous literatures[39,40].

Fig.7b presents the influence of the initial phenol concentration (C_0) on the photocatalytic activity. It can be seen that lower phenol concentration gives a more efficient degradation. A higher phenol concentration of 1.5×10^{-4} M gives a decreased degradation ratio by ca. 20%. It is believed that as the C_0 of phenol increases, the surface active sites of BBN would be over loaded by additional phenol molecules. Resultantly, the photo-generation of reactive oxygen species would be reduced. In addition, more incident photons would be intercepted by increased phenol molecules before they reach and react with the photocatalyst.[41] So 10 mg of BBN per 10 mL phenol solution (10^{-4} M) was fixed to be the optimum photocatalytic parameters.

Photocatalytic mechanism

To evaluate the role of the primary reactive species, scavenger experiments were performed by adding individual scavengers to the phenol/BBN system and the results were shown in Fig. 8. The addition of *tert*-butanol (TBA), a well-known scavenger of •OH radicals,[42] into the photoreaction system causes a decreased degradation efficiency of 16.6% after 45 min irradiation. The weak inhibition indicates that •OH may be not the major species in the oxidation process. However, the introduction of holes scavenger ethylene diamine tetra-acetic acid (EDTA)[42] gives a greatly depressed degradation efficiency of 50.1% at 45 min. And the presence of benzoquinone (BQ), a superoxide radical ($O_2^{-}\cdot$) scavenger,[43] leads to the most strong inhibition for phenol degradation. In addition, the photocatalysis was carried out with continuous N_2-sparging due to the non-volatility of phenol. Under the anoxic condition, the

degradation of phenol is also significantly suppressed. The presence of oxygen is important and its effect is to primarily act as an efficient e^- trap, leading to the generation of $O_2^{-}\cdot$ and preventing the recombination of e^- and h^+.[44,45] The similar results with added BQ and in N_2-saturated suspension together confirm the most important effect of $O_2^{-}\cdot$. Accordingly, the reactive species are believed to play their oxidation roles in a sequence of $O_2^{-}\cdot$, h^+, and •OH in phenol/BBN system.

The photocatalytic oxidation of phenol often involves complicated processes. HPLC was utilized to monitor the evolution of intermediates during phenol degradation over the BBN with dominant {110} facets. Fig.9a-c shows typical HPLC chromatograms of the phenol degradation solutions before and after irradiation for different time. The original solution exhibits only one strong peak at the retention time of 9.5 min corresponding to phenol (Fig. 9a). The intensity of phenol peak decreases gradually with prolonged irradiation and disappears after 45min (Fig. 9b-c), indicating the full degradation of phenol and in good consistence with the results shown in Fig.6a. In addition to the under-degraded phenol, three major aromatic products were detected in the initial stage with retention time of 2.2, 3.1 and 4.6 min, respectively. And the intermediates are identified to be hydroquinone, resorcinol and catechol by contrasting to the chromatogram of standard materials.

The corresponding concentration-time curves calculated from the internal standard calibration with good linear correlation (Tab. S2) were shown in Fig.9d. Accompanied with continuously decreasing concentration of phenol (Fig. S4), the concentration of intermediates all enhances at earlier stage and then reduces quickly. In specific,

catechol and hydroquinone achieve the maximum concentration of 0.00113 and 0.00045 mg/ml at 8 min and resorcinol reaches a peak concentration of only 0.00029 mg/ml at 3 min. According to the substitution rules, ·OH radicals attack the phenol molecules with higher probability in 2 and 4 positions versus OH group of the aromatic ring. So it is rational that the *m*-positioned resorcinol presents a concentration of the minimum. In previous reports on traditional TiO_2, benzoquinone is also a common organic byproduct generated during the degradation of phenol.[46] It is different that no obvious benzoquinone peak is detected in the phenol/BBN system. The O_2^{-}· and h^+ have been ascertained to be the dominant active species, which are nonselective for organic degradation with strong oxidation ability. It may be inferred that the life span of benzoquinone formed at different stages of the reaction is short due to the fast oxidation by O_2^{-}· and h^+. The transient presence of benzoquinone with low concentration would make it difficult to be detected.[24] The aromatic intermediates would undergo further photocatalytic oxidation quickly to form nontoxic aliphatic acids by ring cleavage[47]and subsequently be completely transformed to CO_2 and H_2O.

It is well known that the effective separation and transfer of photoinduced electrons and holes are important factors for a desired photocatalyst. And the key to cause the migration of carriers is the difference between the redox potential of active species and the positions of valence band (VB) and conduction band (CB) of the semiconductor. Combined the band edges of BBN with the ascertained oxidative species, a proposed migration mechanism of photogenerated carriers on the surface of BBN is illustrated in Fig.10. The BBN is excited by UV irradiation to generate

electrons in CB and holes in VB, which then migrate to the surface of photocatalyst. It is reported that BBN exhibits *n*-type characteristics with CB potential at -0.90 V,[22] which is more negative than the redox potential of $O_2/O_2^{-\cdot}$ (-0.28V *vs.* NHE).[48] Then forced by the potential difference, the CB electrons can be quickly captured by the adsorbed molecular oxygen in water to form $O_2^{-\cdot}$, which has been confirmed to be the most important active species. While the VB holes are believed to play vital roles through two different routes at the phenol/BBN interface. The major one is the direct degradation to phenol due to the strong oxidative ability of BBN holes with calculated VB position of 2.40 V based on the estimated *Eg* of 3.3 eV in DRS spectra. And the direct oxidation has been affirmed by the greatly inhibited degradation efficiency with added EDTA. In addition, the hole can also oxidize the OH^- or H_2O in phenol solution to form •OH owing to the slightly anodic VB position compared with the redox potential of $•OH/OH^-$ (2.38 V *vs.* NHE).[49] And •OH has also been confirmed to be one of the active species in phenol/BBN although not the most important. Then the •OH invades into phenol molecules in the initial stage of photocatalysis, leading to the formation of benzenediol intermediates as monitored by HPLC. Then with the synergism of active species of $O_2^{-\cdot}$, h^+, and •OH, the phenol and intermediates would subsequently decomposed into nontoxic alphatic acids[47,50] and finally transformed to H_2O and CO_2.

4. Conclusions

In summary, the BBN photocatalyst $Bi_6O_6(OH)_3(NO_3)_3 \cdot 1.5H_2O$ with predominately exposed {110} facets was selectively prepared. The sample exhibit much higher

photocatalytic activities to phenol than that of BBN with dominant {001} planes and commercial P25 with rate constants *k* improved by 3.6 and 2.8 folds, respectively. It suggests that {110} facets should be the reactive high-energy crystal planes in BBN. And the work provides a better understanding of the correlation among preparation parameter, specific structure and photocatalytic performance of the novel photocatalyst. The scavenger experiments and HPLC technique disclose the dominant active species and main intermediates in the initial stage of photocatalysis. And the possible migration mechanism of photogenerated carriers on the surface of BBN is proposed.

Acknowledgements

The project was supported by National Natural Science Foundation of China (No. 21303122), the Program for Innovative Research Team in University of Tianjin (TD12-5038), and the Open Project Program of Tianjin Key Laboratory of Structure and Performance for Functional Molecules in 2014.

References

1 L. H. Keith and W. A. Telliand, *Environ. Sci. Technol.*, 1979, 13, 416-423.

2 F. J. Diaz, A. T. Chow, A. T. O'Geen, R. A. Dahlgren and P. K. Wong, *Water Res.*, 2009, 43, 2750-2760.

3 M. R. Hoffmann, S. T. Martin, W. Choi and D. W. Bahnemann, *Chem. Rev.*, 1995, 95, 69-96..

4 S. W. Liu, J. G. Yu and M. Jaroniec, *J. Am. Chem. Soc.*, 2010, 132, 11914-11916.

5 M. Mecklenburg, A. Schuchardt, Y. K. Mishra, S. Kaps, R. Adelung, A. Lotnyk, L.

Kienle and K. Schulte, *Adv. Mater.*, 2012, 24, 3486–3490.

6 G. W. Cui, W. L. Wang, M. Y. Ma, M. Zhang, X. Y. Xia, F. Y. Han, X. F. Shi, Y. Q Zhao, Y. B. Dong and B. Tang, *Chem. Commun.*, 2013, 49, 6415-6417.

7 J. W. Tang, Z. G. Zou and J. H. Ye, *Angew. Chem. Int. Ed.*, 2004, 43, 4463-4466.

8 L. Zhang, W. Wang, J. Yang, Z. Chen, W. Zhang, L. Zhou and S. Liu, *Appl. Catal. A.*, 2006, 308, 105-110.

9 X. Xiao, R. P. Hu, S. H. Tu, C. X. Zheng, H. Zhong, X. X. Zuo and J. M. Nan, *RSC Adv.* 2015, 5, 38373-38381.

10 F. Amano, A. Yamakata, K. Nogami, M. Osawa and B. Ohtani, *J. Am. Chem. Soc.*, 2008, 130, 17650-17651.

11 L.S. Zhang, H. L. Wang, Z. G. Chen, P. K. Wong and J. S. Liu, *Appl. Catal. B.*, 2012, 47, 1919-1924.

12 G. Tian, Y. Chen, W. Zhou, K. Pan, Y. Dong, C. Tian and H. Fu, *J. Mater. Chem.*, 2011, 21, 887-892.

13 M. Zhang, C. Shao, P. Zhang, C. Su, X. Zhang, P. Liang, Y. Sun and Y. Liu, *J. Hazard. Mater.*, 2012, 225-226, 155-163.

14 D. Tang, H. C. Zhang, H. Huang, R. H. Liu, Y. Z. Han, Y. Liu, C. Y. Tong and Z. H. Kang, *Dalton Trans.*, 2013, 42, 6285-6289.

15 D. Ke, T. Peng, L. Ma, P. Cai and K. Dai, *Inorg. Chem.*, 2009, 48, 4685-4691.

16 Y. Xu, S. C. Xu, S. Wang, Y. X. Zhang and G. H. Li, *Dalton Trans.*, 2014, 43, 479-485.

17 J. Xiong, Q. Dong, T. Wang, Z. Jiao, G. Lu and Y. Bi, *RSC Adv.*, 2014, 4,

583-586.

18 R. Hao, X. Xiao, X. Zuo, J.M. Nan and W. D. Zhang, *J. Hazard. Mater.*, 2012, 209-210, 137-145.

19 N. Henry, M. Evain, P. Deniard, S. Jobic, O. Mentré and F. Abraham, *J. Solid State. Chem.*, 2003, 176, 127-136.

20 N. Henry, O. Mentre, J.C. Boivin and F. Abraham, *Chem. Mater.*, 2001, 13, 543-551.

21 L. Y. Xie, J. X. Wang, Y. H. Hu, Z. Y. Zheng, S. X. Weng and P. Liu, *Mater. Chem. Phys.*, 2012, 136, 309-312.

22 L. Y. Xie, J. X. Wang, Y. H. Hu, S. Y. Zhu, Z. Y. Zheng, S. X. Weng and P. Liu, *RSC Adv.*, 2012, 2, 9881-9886.

23 Y. Cui, L. M. Yang, G. Y. Zhang and Y. Feng, *Catal. Commun.* 2015, 59, 83-87.

24 Y. X. Yang, H. Y. Liang, N. Zhu, Y. P. Zhao, C. S. Guo and L. Liu, *Chemosphere.*, 2013, 93, 701-707.

25 S. He, S. Zhang, J. Lu, Y. Zhao, J. Ma, M. Wei, D. G. Evans and X. Duan, *Chem. Commun.*, 2011, 47, 10797-10799.

26 Z. Y. Jiang, Q. Kuang, Z. X. Xie and L. S. Zheng, *Adv. Funct. Mater.*, 2010, 20, 3634-3645.

27 Z. Y. Zhou, N. Tian, J. T. Li, I. Broadwell and S. G. Sun, *Chem. Soc. Rev.*, 2011, 40, 4167-4185.

28 H. G. Yang, C. H. Sun, S. Z. Qiao, J. Zou, G. Liu, S. C. Smith, H. M. Cheng and G. Q. Lu, *Nature* 2008, 453, 638-641.

29 G. Liu, H. G. Yang, X. Wang, L. Cheng, J. Pan, G. Q. Lu and H. M. Cheng, *J. Am. Chem. Soc.*, 2009, 131, 12868-12869.

30 J. Jiang, K. Zhao, X. Y. Xiao and L. Z. Zhang, *J. Am. Chem. Soc.*, 2012, 134, 4473-4476.

31 Y. Xu, S. C. Xu, S. Wang, Y. X. Zhang and G. H. Li, *Dalton Trans.*, 2014, 43, 479-485.

32 A. N. Christensen, M. A. Chevallier, J. Skibsted and B. B. Iversen, *J. Chem. Soc., Dalton Trans.*, 2000, 265-270.

33 Z. Chen, L. W. Qian, J. Zhu, Y. P. Yuan and X. F. Qian, *CrystEngComm.*, 2010, 12, 2100-2106.

34 A. Kudo, I. Tsuja and H. Kato, *Chem. Commun.*, 2002, 1958-1959.

35 Y. Ohko, K. Hashimoto and A. Fujishima, *J. Phys. Chem. A.*, 1997, 101, 8057-8062.

36 J. Zhang, F. J. Shi, D. F. Chen, J. M. Gao, Z. X. Huang, X. X. Ding and C. C. Tang, *Chem. Mater.*, 2008, 20, 2937-2941.

37 C. X. Li, Y. T. Li and Z. H. Wang, *J. Environ. Eng-China.*, 2002, 8, 48-51.

38 M. A. Gondal, X. F. Chang and Z. H. Yamani, *Chem. Eng. J.*, 2010, 165, 250-257.

39 X. Chang, G. Ji, Q. Sui and J. Huang, *J. Hazard. Mater.*, 2009, 166, 728-733.

40 G. Y. Zhang, Y. Feng, Y. Y. Xu, D. Z. Gao and Y. Q. Sun, *Mater. Res. Bull.,* 2012, 47, 625-630.

41 I. K. Konstantinou and T. A. Albanis, *Appl. Catal. B.*, 2004, 49, 1-14.

42 H. J. Lu, L. L. Xu, B. Wei, M. Y. Zhang, H. Gao and W. J. Sun, *J. Appl. surf. Sci.*,

2014, 303, 360-366.

43 M. Ge, N. Zhu, Y. P. Zhao, J. Li and L. Liu, *Ind. Eng. Chem. Res.,* 2012, 51, 5167-5173.

44 Z. J. Zhang, W. Z. Wang, E. P. Gao, M. Shang and J. H. Xu, *J. Hazard. Mater.*, 2011, 196, 255-262.

45 H. B. Fu, C. S. Pan, W. Q. Yao and Y. F. Zhu, *J. Phys. Chem. B.*, 2005, 109, 22432-22439.

46 L. Liu, H. J. Liu, Y. P. Zhao, Y. Q. Wang, Y. Q. Duan, G. D. Gao, M. Ge, and W. Chen, *Environ. Sci. Technol.*, 2008, 42, 2342-2348.

47 Z. Deng, C. Zhang and Lin Liu, *Intermetallics.*, 2014, 52, 5-14.

48 Y. L. Zhang, D. Y. Li, Y. G. Zhang, X. F. Zhou, S. J. Guo and L. B. Yang, *J. Mater. Chem. A.*, 2014, 2, 8273-8280.

49 Y. Y. Liu, Z. Y. Wang, B. B. Huang, X. Y. Zhang, X. Y. Qin and Y. Dai, *J. Colloid Interf. Sci*., 2010, 348, 211-215.

50 X. Y. Li, Y. H. Cui, Y. J. Feng, Z. M. Xie and D. Gu, *J. Water Res.*, 2005, 39, 1972-1981.

Figure captions:

Fig. 1 XRD pattern of the as-synthesized BBN sample and the bottom is the JCPDS standard.

Fig. 2 (a) Panoramic FE-SEM image of the product, (b) magnified FE-SEM image, (c)

TEM image of an isolated structure, (d) HRTEM image of the edge part in c, and (e) the corresponding SAED pattern.

Fig. 3 SEM images and XRD patterns of time series samples: (a) precursor, (b) 30 min, (c) 50 min, (d) 2 h, and (e) 8 h.

Fig. 4 SEM images and XRD patterns of temperature series samples: (a) 80°C, (b) 100°C, (c) 120°C, (d) 160°C, (e) 200°C, and (f) corresponding XRD patterns.

Fig. 5 UV-vis diffuse reflectance spectrum of BBN sample with *Eg* analysis in inset.

Fig. 6 Photocatalytic degradation of phenol and corresponding pseudo first-order plots over: (a, b) temperature series samples, and (c, d) time series samples.

Fig. 7 The degradation of phenol over BBN under different operating conditions: (a) BBN dosage, (b) the initial concentration of phenol.

Fig. 8 Photocatalytic degradation of phenol over BBN with the addition of scavengers of different reactive species and in N_2-saturated solutions.

Fig. 9 (a-c) HPLC chromatograms of phenol photodegradation by BBN for different time, (d) concentrations of intermediates formed from phenol during the photocatalysis.

Fig.10 Schematic illustration of the charge transfer on the BBN surface and the degradation process of phenol

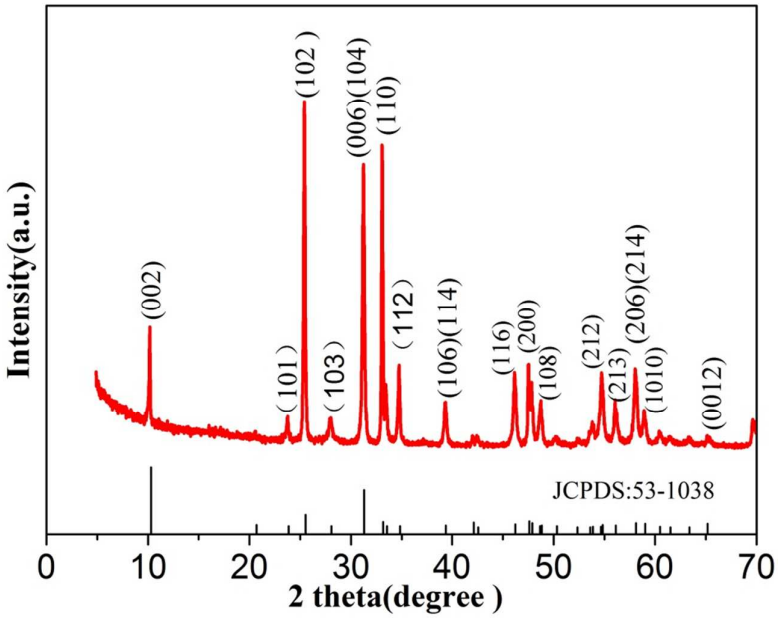

Fig.1

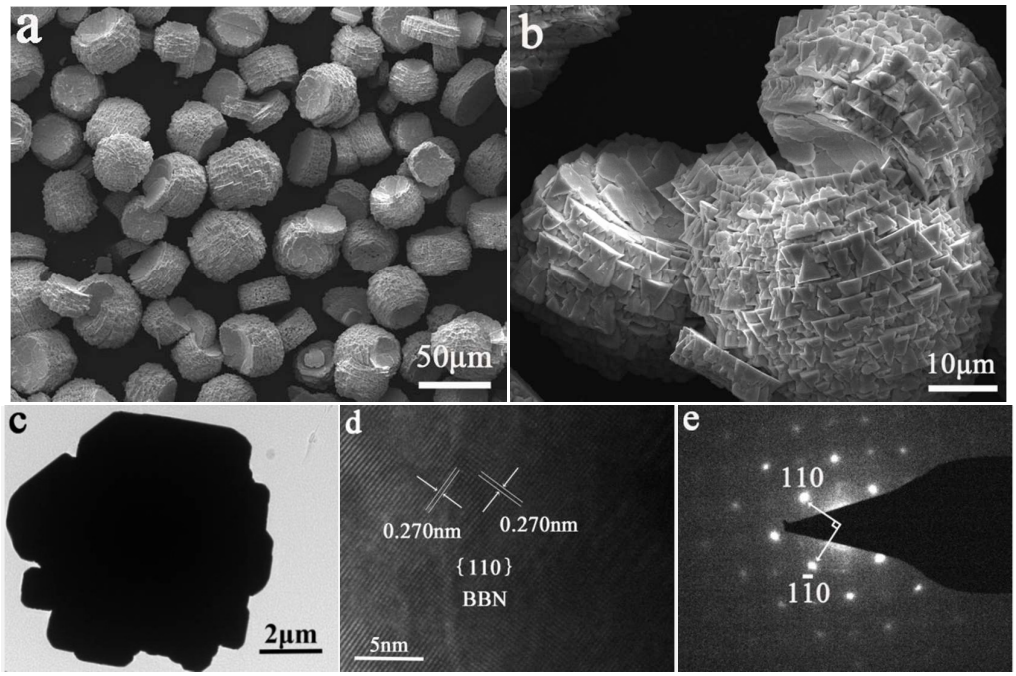

Fig.2

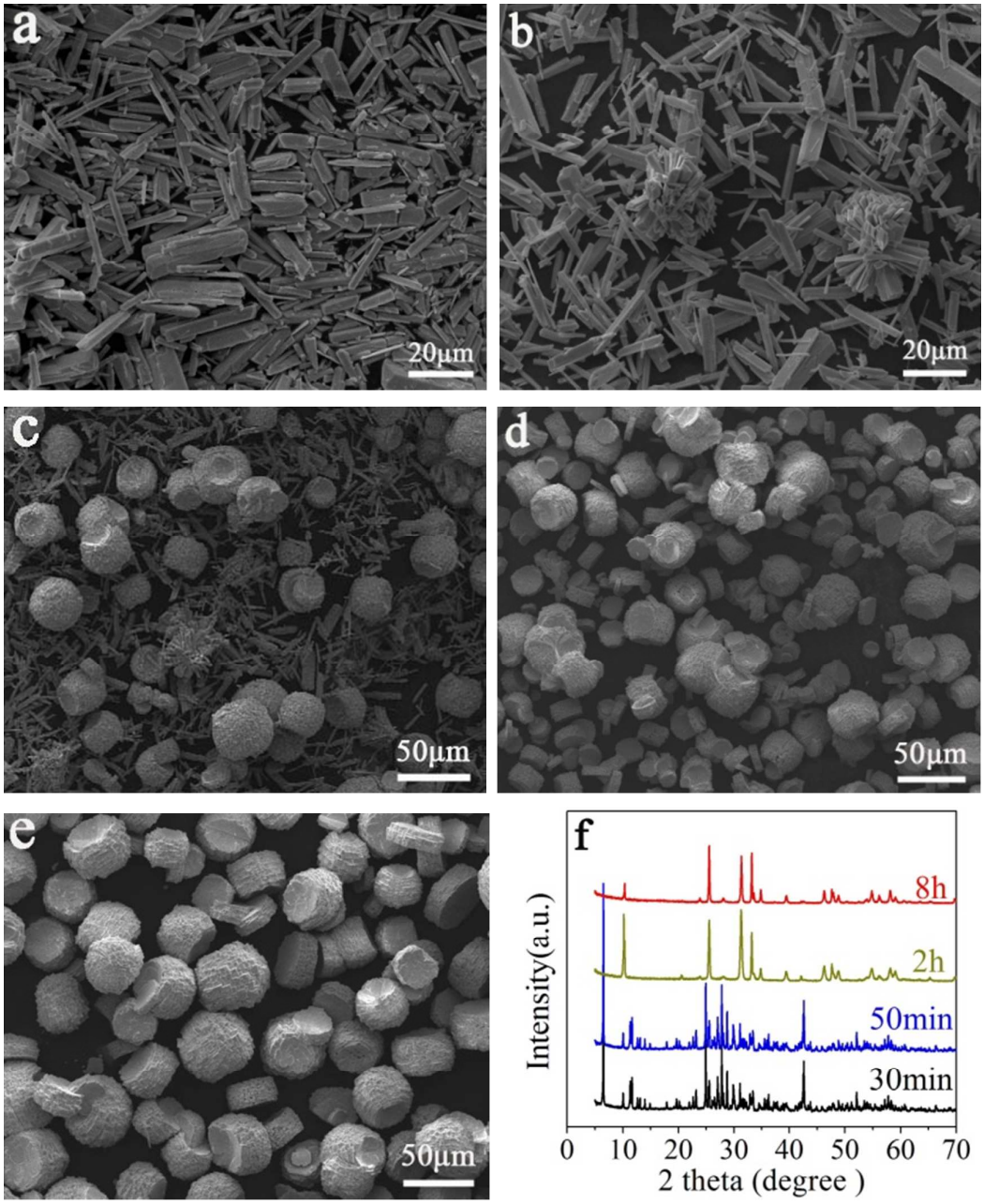

Fig.3

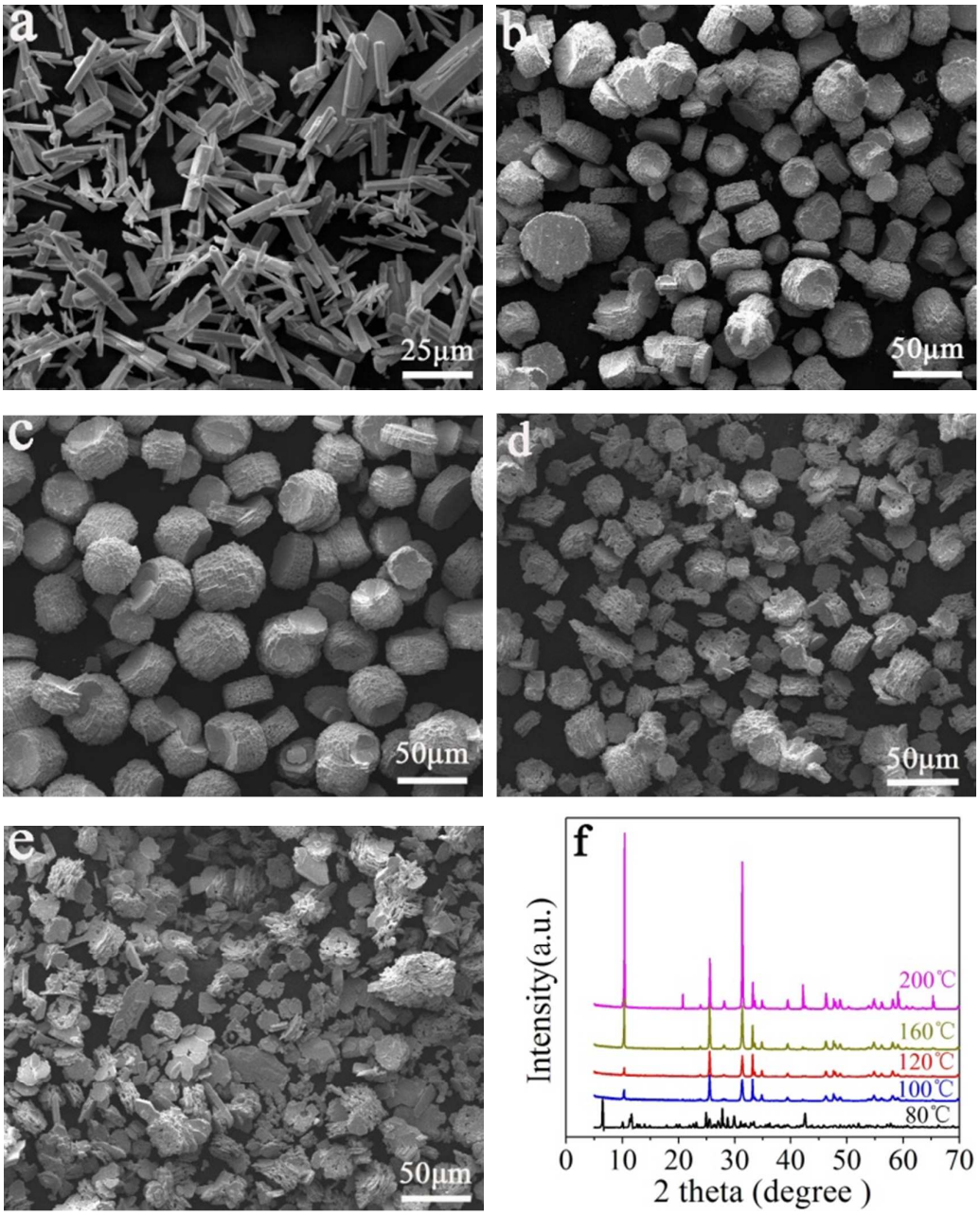

Fig.4

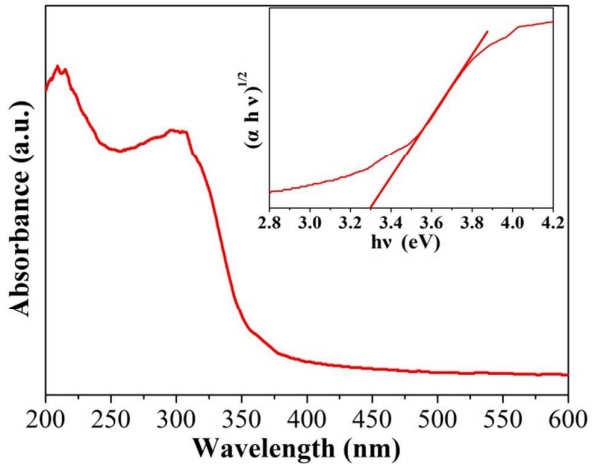

Fig.5

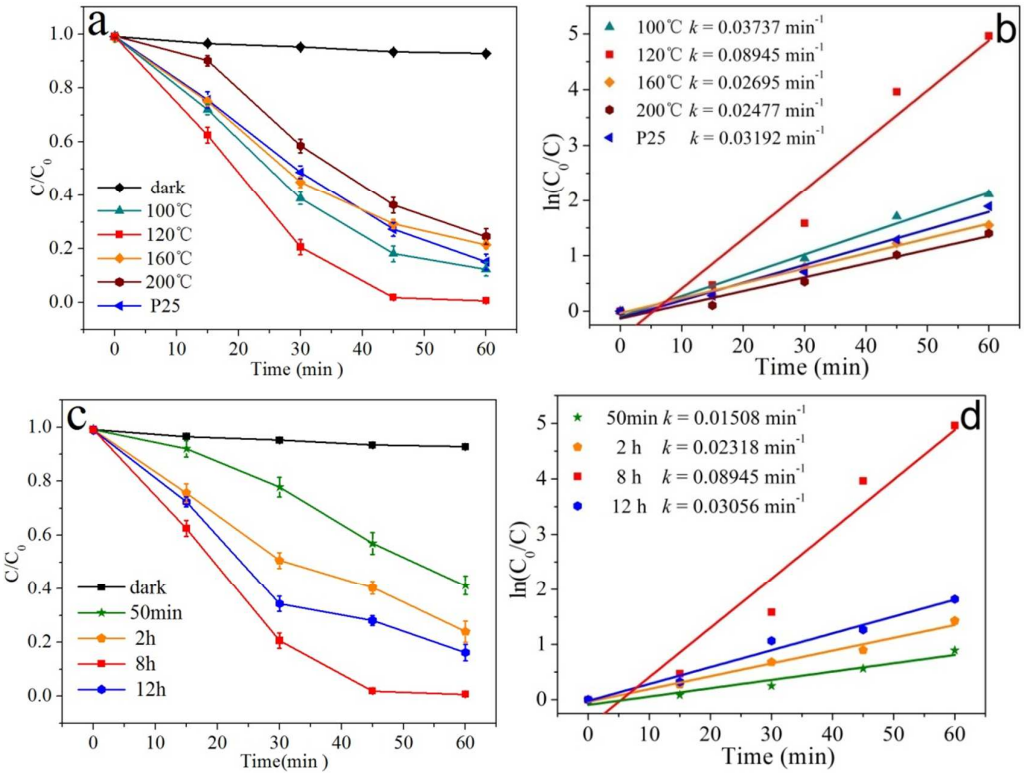

Fig.6

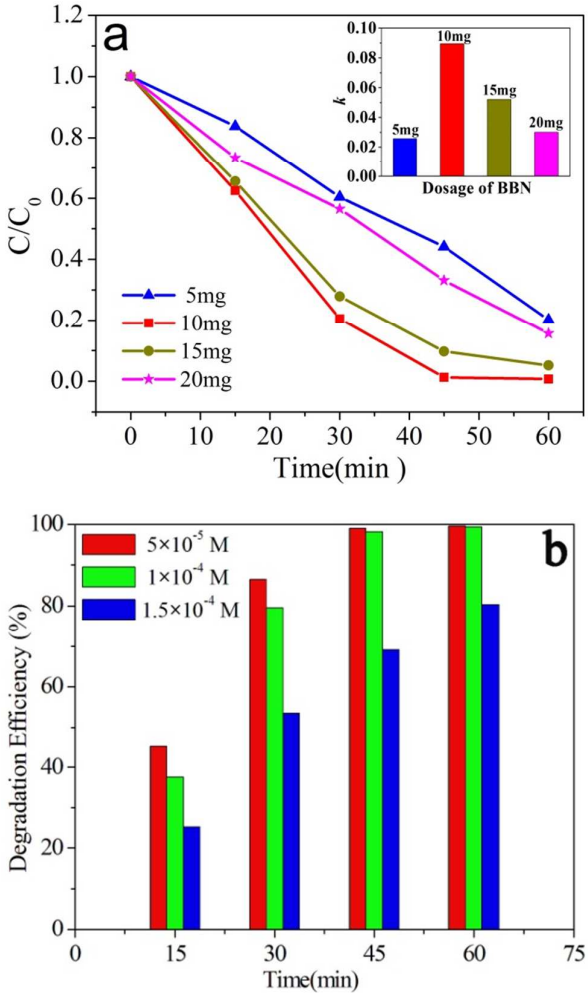

Fig.7

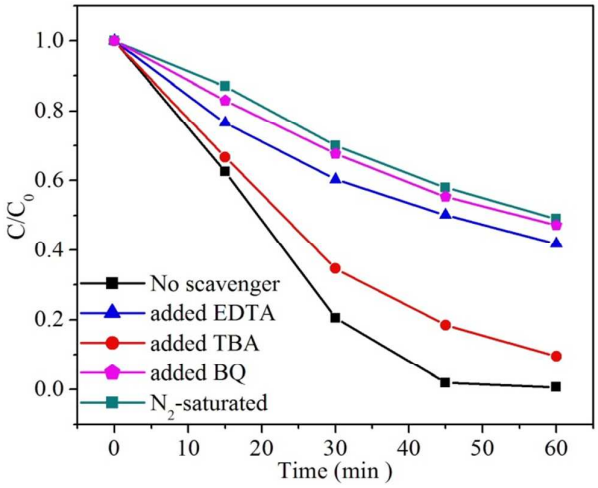

Fig.8

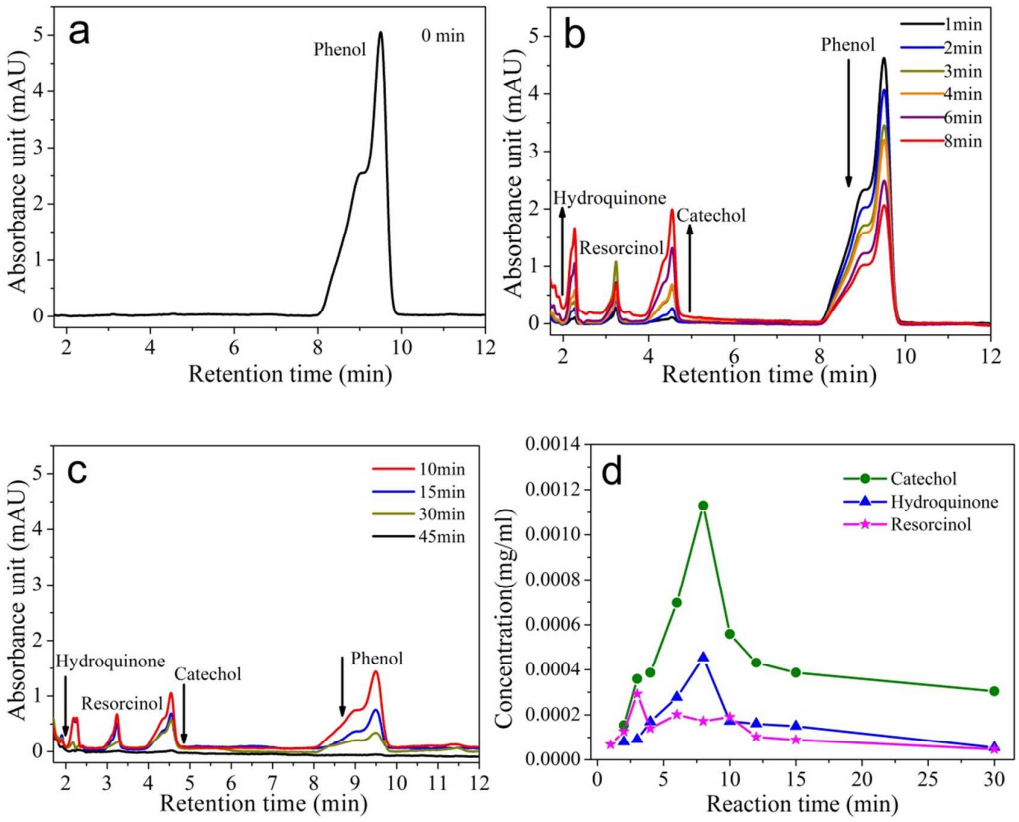

Fig.9

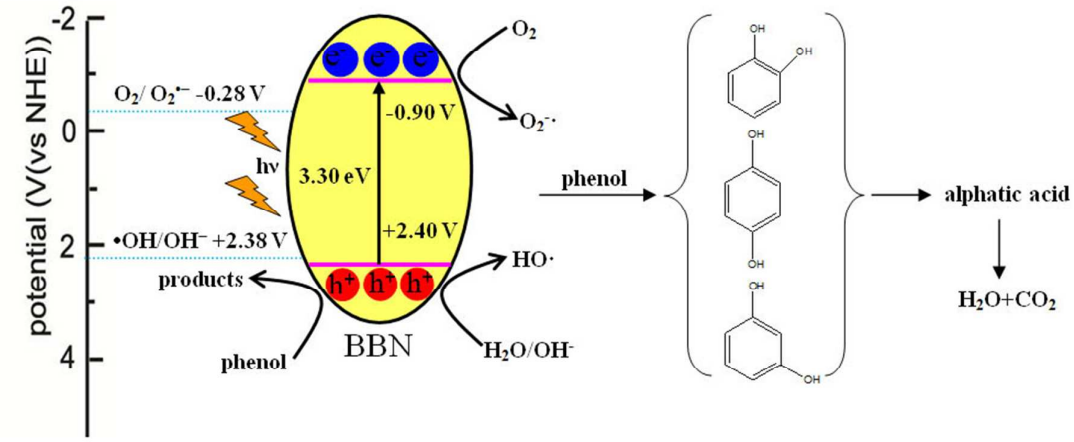

Fig.10

Graphical Abstract

{110} facets predominated $Bi_6O_6(OH)_3(NO_3)_3 \cdot 1.5H_2O$ photocatalyst: selectively hydrothermal synthesis and superior photocatalytic activity for degradation of phenol

Li-Min Yang, Guo-Ying Zhang*, Yue Liu*, Yan-Yan Xu, Chun-Mei Liu, and Jing-Wang Liu

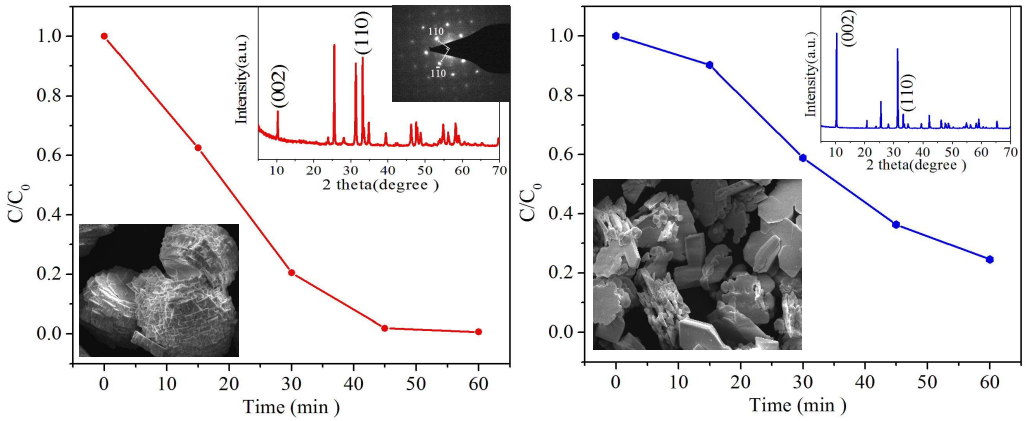

The $Bi_6O_6(OH)_3(NO_3)_3 \cdot 1.5H_2O$ photocatalyst with predominated {110} facets but low BET surface area was selectively prepared. It exhibits much higher photocatalytic activities for degradation of phenol than that of BBN with dominant {001} planes and P25 with rate constants *k* improved by 3.6 and 2.8 folds, respectively, indicating the highly reactive {110} facets in BBN.